Journal of Materials Chemistry A

PAPER

View Article Online
View Journal | View Issue

Cite this: J. Mater. Chem. A, 2016, 4, 8750

Facile synthesis of a hole transporting material with a silafluorene core for efficient mesoscopic $CH_3NH_3PbI_3$ perovskite solar cells†

Anurag Krishna,[a] Dharani Sabba,[b] Jun Yin,[d] Annalisa Bruno,[b] Liisa J. Antila,[e] Cesare Soci,[d] Subodh Mhaisalkar*[bc] and Andrew C. Grimsdale*[bc]

Received 29th February 2016
Accepted 4th May 2016

DOI: 10.1039/c6ta01776b

www.rsc.org/MaterialsA

A novel electron-rich small-molecule, 4,4′-(5,5-dihexyl-5*H*-dibenzo[*b*,*d*]silole-3,7-diyl)bis(*N*,*N*-bis(4-methoxyphenyl)aniline) (S101), containing silafluorene as the core with arylamine side groups, has been synthesized *via* a short efficient route. When S101 was incorporated into a $CH_3NH_3PbI_3$ perovskite solar cell as a hole transporting material (HTM), a short circuit photocurrent density (J_{sc}) of 18.9 mA cm^{-2}, an open circuit voltage (V_{oc}) of 0.92 V, and a fill factor (FF) of 0.65 contributing to an overall power conversion efficiency (PCE) of ~11% which is comparable to the PCE obtained using the current state-of-the-art HTM 2,2′,7,7′-tetrakis(*N*,*N*′-di-*p*-methoxyphenylamine)-9,9′-spirobifluorene (spiro-OMeTAD) (η = 12.3%) were obtained. S101 is thus a promising HTM with the potential to replace the expensive spiro-OMeTAD due to its comparable performance and much simpler and less expensive synthesis route.

In recent years, organic–inorganic metal halide perovskites, in particular methylammonium lead iodide ($CH_3NH_3PbI_3$), have emerged as very promising light harvesting materials for high performance and low cost photovoltaic technology.[1–3] Methylammonium lead halide perovskites have properties such as excellent ambipolar mobility, large exciton diffusion lengths, high extinction coefficients, direct bandgap and excellent absorption throughout the UV-Vis-NIR spectrum which make them excellent light harvesting materials.[4–7] Since the reports of an efficient solid state photovoltaic device using a perovskite as a light absorber by Grätzel, Park *et al.*[2] and Snaith *et al.*,[1] the growth in efficiencies has been unprecedentedly rapid so that a certified PCE of 20.1% has recently been reported.[8–10] A typical solid state perovskite solar cell comprises a nanocrystalline mesoporous TiO_2 anode, a perovskite absorbing layer, a hole transporting layer and a metallic counter electrode. In addition to the quality of the perovskite film, the performance of perovskite solar cells is also strongly affected by the use of charge transporting layers, with high efficiencies only being obtained when using an HTM. In spite of the high price of spiro-OMeTAD, which is due to its multistep low yielding synthesis and difficult and expensive purification process, it is the most widely used HTM for perovskite based solar cells, as it has produced the highest device efficiencies to date. However, there has been a concerted research effort to design and synthesize alternative HTMs, which are more economical and show device performance comparable to that of spiro-OMeTAD.[4,11] Several solution processable conjugated polymers including P3HT and poly(triarylamine) (PTAA) have been employed as HTMs; however their device results to date have been markedly inferior to that of spiro-OMeTAD.[12] A number of small molecule HTMs based on ethylenedioxythiophene,[13] cruciform oligothiophenes,[14] pyrene,[15] triptycene,[16] triazines,[17] conjugated quinolizino acridine,[18] carbazole,[19] planar triphenylamine[20] furan,[21] silolothiophene,[22] methoxydiphenylamine-substituted carbazole,[23] tetrathiafulvalene,[24] phenoxazine,[25] po-spiro-OMeTAD,[26] spiro-thiophene[27], [2,2]paracyclophane[28] and ethene-tetraarylamine[29] cores have also been reported. The best performing HTMs show similar or superior performance to spiro-OMeTAD in some aspects but no material has yet emerged clearly superior in all aspects of device performance, particularly in terms of cost, device efficiency and stability. Hence it remains a key challenge to make simple, cost effective and high performance HTMs.

The present study reports a novel HTM S101 (Fig. 1) based on an electron rich silafluorene core. Silole and its derivatives have been widely used in organic electronics because of their excellent properties including good redox stability in air and high

[a]Energy Research Institute, Interdisciplinary Graduate School, Nanyang Technological University, Singapore, Singapore

[b]Energy Research Institute@NTU (ERI@N), Research Techno Plaza, X-Frontier Block, Level 5, 50 Nanyang Drive, 637553, Singapore, Singapore. E-mail: acgrimsdale@ntu.edu.sg

[c]School of Materials Science and Engineering, Nanyang Technological University, Nanyang Avenue, 639798, Singapore, Singapore

[d]Division of Physics and Applied Physics, Nanyang Technological University, 21 Nanyang Link, Singapore 637371, Singapore

[e]Department of Chemistry – Angström Laboratory, Uppsala University, Lägerhyddsvägen 1, 75120 Uppsala, Sweden

† Electronic supplementary information (ESI) available: Experimental details, spectra, results of crystal packing simulations and analysis of manufacturing costs for S101 and spiro_OMeTAD. See DOI: 10.1039/c6ta01776b

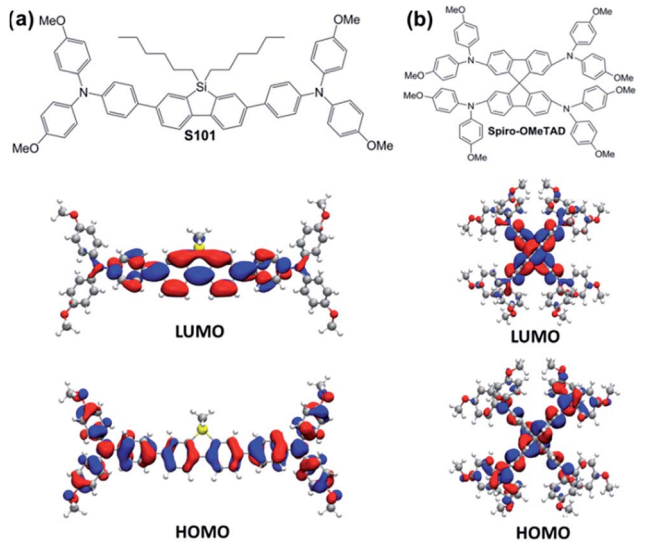

Fig. 1 (a) Chemical structure of S101 and electronic density distribution of the lowest unoccupied molecular orbital (LUMO) and highest occupied molecular orbital (HOMO) for S101; (b) chemical structure of spiro-OMeTAD and electronic density distribution of the LUMO and HOMO for spiro-OMeTAD.

charge carrier mobilities.[30–32] In this work, an electron rich silafluorene is used as the core, to which are linked hole-accepting triphenylamine moieties, while hexyl chains are attached to the silicon atom to produce high solubility in organic solvents and so improve processability. The S101 molecule has a planar structure which is desirable for promoting intramolecular π-delocalization and intermolecular π–π stacking, which favour both charge carrier mobility and lifetime, boosting device efficiency.[33] Silafluorene core based materials have also been used in organic light emitting diodes.[34] S101 was synthesized from a relatively inexpensive commercially available silafluorene derivative in a single step with an acceptable yield (45%). In addition to extensive investigation of its material properties, we have also investigated the performance of S101 in mesoscopic perovskite solar cells in terms of *I–V* characteristics and charge carrier dynamics. The devices fabricated using S101 demonstrated efficiency ∼11% which is comparable to the values obtained using the state-of-the-art HTM spiro-OMeTAD.

Fig. 1 shows the chemical structure of the S101 and spiro-OMeTAD together with the electronic density distribution of their frontier orbitals calculated by density functional theory (DFT). For S101, the highest occupied molecular orbital (HOMO) level shows a π-bonding character, spreading over the whole molecule, while the lowest unoccupied molecular orbital (LUMO) shows a π*-antibonding character being predominately localized on the central silafluorene and two benzene units. The calculated HOMO energy of S101 (−4.49 eV) is quite close to that of spiro-OMeTAD (−4.48 eV), which would promote effective hole transfer from the perovskite to S101.

The hole transfer rate of hole-transporting materials can be described by the Marcus–Hush equation which is dominated by two important parameters, namely, (1) reorganization energy and (2) electronic coupling, which can be obtained from DFT calculations (see the Computational methods in the ESI†). Fig. S1 (ESI†) demonstrates the predicted crystal structures of S101 and spiro-OMeTAD with all possible hole-hopping pathways. The molecular structure of S101, with a planar silafluorene core, has much smaller intermolecular distances, resulting in larger electronic coupling between HOMO levels of neighbouring molecules, which can improve the hole transporting mobility (see Table S1 and S2 in the ESI†). S101 shows smaller hole reorganization energy (0.13 eV) than spiro-OMeTAD (0.15 eV) and predicted hole mobilities for the simulated charge transport pathways (0.215, 0.141, and 0.049 $cm^2 V^{-1} s^{-1}$) which are one order of magnitude higher than those of spiro-OMeTAD (0.0058, 0.0046, and 0.0532 $cm^2 V^{-1} s^{-1}$). These values are comparable with those of our previously synthesized high performance furan-based HTM F101,[21] showing that S101 is also a promising HTM with potentially relatively high hole mobility.

Together with its predicted material properties, the short relatively efficient synthesis route of S101 makes it an attractive HTM for any potential perovskite solar cell industry. The synthesis route of S101 (Scheme 1) is shorter and less expensive as compared to that of spiro-OMeTAD (see Scheme S1 and Table S4 in the ESI† for the analysis of relative synthesis costs). The commercially available relatively inexpensive 3,7-dibromo-5,5-dihexyl-5*H*-dibenzo[*b*,*d*]silole was Suzuki coupled with a triphenylamine boronic acid derivative[35] to give S101 in 45% yield from an unoptimised reaction. NMR spectroscopy and MALDI-TOF mass spectrometry confirmed the molecular structure of S101.

The optoelectronic properties of S101 have been systematically investigated and compared with those of spiro-OMeTAD. In the UV-Vis absorption spectra (shown in Fig. 2a), absorption peaks of S101 and spiro-OMeTAD were observed at 381 nm and 384 nm, respectively. The absorption onset wavelengths of S101 and spiro-OMeTAD are 434 nm and 420 nm, respectively, which correspond to band gaps of 2.86 eV and 2.95 eV, respectively. The onset of absorption in S101 is slightly red shifted with respect to that in spiro-OMeTAD which can be attributed to the more extended conjugation in the backbone of S101 due to the presence of two extra phenyl rings between the nitrogens. From the cyclic voltammograms of S101 and spiro-OMeTAD, shown in Fig. 2b, the pair of redox peaks for S101 is observed to be highly reversible, showing that it has excellent electrochemical stability. The HOMO energy level was calculated from the CV data using the following equation: $E_{HOMO} = -5.1 - (E_{ox,HTM}$ *vs.* $Fc/Fc^+)$ (eV), where $E_{ox,HTM}$ *vs.* Fc/Fc^+ is the onset of oxidation potential of ferrocene, which is used as the reference and −5.1 eV is the redox potential of ferrocene.[36] The HOMO levels

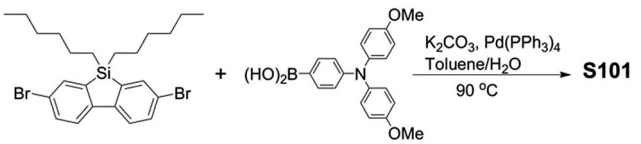

Scheme 1 Synthesis route of S101.

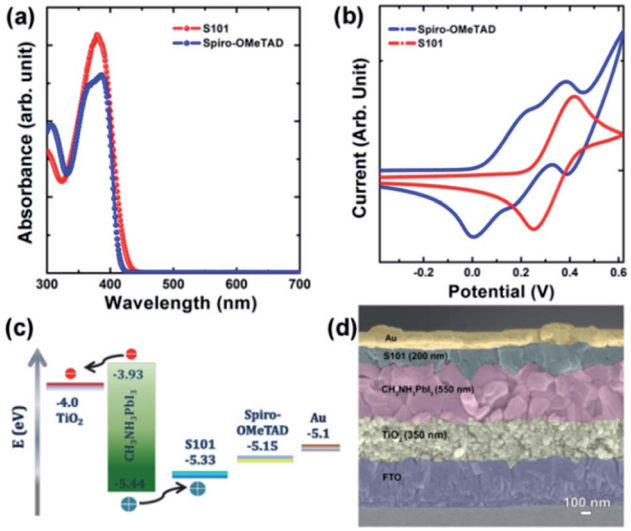

Fig. 2 (a) Absorption spectra of spiro-OMeTAD and S101, (b) cyclic voltammograms of spiro-OMeTAD and S101, (c) band diagram of the device with new HTM S101 and spiro-OMeTAD, and (d) cross-sectional SEM image of the device fabricated with S101.

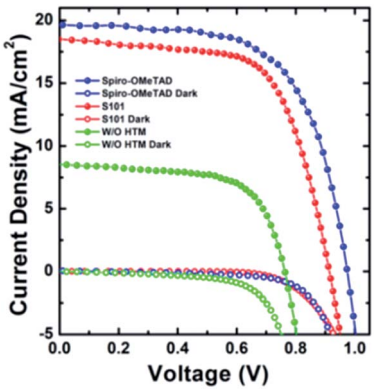

Fig. 3 Current density *vs.* voltage curve under AM 1.5G illumination (100 mW cm^{-2}).

of S101 and spiro-OMeTAD as calculated from CV are 5.32 eV and 5.15 eV, respectively, while the reported HOMO energy level of $CH_3NH_3PbI_3$ is 5.44 eV[2] which indicates that S101 has favourable energetics for the hole transfer (Fig. 2c). The energetics of the system employing S101/spiro-OMeTAD are presented in Fig. 2c and Table 1 summarizes the optical and electrochemical properties of the two HTMs. Differential scanning calorimetry (DSC) showed that S101 has a weak glass transition (T_g) at 45 °C and a melting point (T_m) of 143 °C (see Fig. S5 in the ESI†); *cf.* T_g = 124 °C and T_m = 245 °C for spiro-OMeTAD. The cross-sectional scanning electron microscopy (SEM) images shown in Fig. 2d display the various interfaces of the S101 HTM based $CH_3NH_3PbI_3$ solar cell indicating that we have achieved the formation of a well-defined hybrid structure with clear interfaces. From the FE-SEM image, the thicknesses of the TiO_2, perovskite and the HTM layers can be estimated to be ~350, 550 and 200 nm, respectively. To investigate the charge-carrier mobility of S101 and spiro-OMeTAD, field effect transistors were fabricated. To determine the charge carrier mobility, field effect transistors (FETs) were fabricated using spiro-OMeTAD and S101. Hole mobilities evaluated from FET transfer characteristics (shown in Fig. S6 in the ESI†) are 1.2×10^{-4} cm^2 V^{-1} s^{-1} (at $V_d = -50$ V; $V_g = -40$ V) for spiro-OMeTAD, and 7.2×10^{-5} cm^2 V^{-1} s^{-1} (at $V_d = -50$ V; $V_g = -40$ V) for S101. Contrary to the predictions, Spiro-OMeTAD thus has slightly higher field-effect mobility than S101, which suggests that spiro-OMeTAD based devices should show slightly higher fill factors.

The current–voltage (*J*–*V*) characteristics of perovskite solar cells employing S101 and spiro-OMeTAD as HTMs, together with devices without HTMs, are shown in Fig. 3 and summarized in Table 2. The PCEs of the best performing device with S101 and spiro-OMeTAD as the HTM are 11% and 12.3%, respectively. Our study also showed that the device fabricated without a HTM had a PCE of only around 4.7%, which confirmed that a HTM must be an integral component of high efficiency perovskite solar cells. The short circuit current densities (J_{sc}) of the cells fabricated using spiro-OMeTAD and S101 are 19.7 mA cm^{-2} and 18.9 mA cm^{-2}, respectively. The slightly higher current using spiro-OMTAD can be attributed to its higher HOMO level as compared to that of S101, which gives spiro-OMeTAD a higher driving force for charge transfer from the perovskite to the HTM. The devices fabricated with both HTMs exhibit similar fill factors. The devices with S101 showed a slightly lower open circuit voltage (V_{oc} = 0.92 V) than devices employing spiro-OMeTAD (V_{oc} = 0.975 V). However, from our CV data, it is observed that the HOMO energy level of S101 is deeper than that of spiro-OMeTAD which should result in higher V_{oc}. As the V_{oc} depends on (1) the splitting of the Fermi levels for photogenerated charges, (2) the recombination, and (3) the energetics of the devices,[15,16,21] the slightly lower voltage in devices fabricated with S101 as the HTM might be due to high

Table 1 Optical and electrochemical properties of S101 and spiro-OMeTAD

HTM	λ_{max} (nm)	λ_{onset} (nm)	E_g[a] (eV)	E_{HOMO} (eV)	E_{LUMO}[b] (eV)
S101	381	434	2.86	−5.32	−2.46
Spiro-OMeTAD	384	420	2.95	−5.15	−2.2

[a] Optical band gap (E_g) obtained from the onset value of absorption (λ_{onset}). [b] LUMO calculated by LUMO = HOMO + E_g.

Table 2 Summary of device parameters; open circuit voltage (V_{oc}), current density (J_{sc}), fill factor (FF) and efficiency (η). Area = 0.2 cm^2

HTM	J_{sc} (mA cm^{-2})	V_{oc} (V)	FF (%)	η_{max} (%)	η_{avg}[a] (%)
S101	18.9	0.92	65	11	10.6
Spiro-OMeTAD	19.7	0.975	64.2	12.3	12.0
W/O HTM	8.54	0.76	72	4.7	4.3

[a] Average PCE is based on six cells in a single batch.

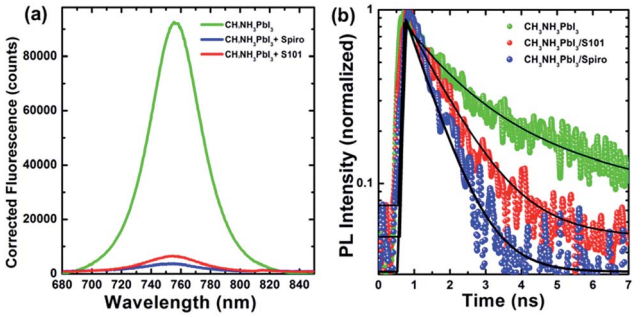

Fig. 4 (a) The steady-state photoluminescence (PL) spectra and (b) time-resolved PL spectra of $CH_3NH_3PbI_3$, $CH_3NH_3PbI_3$/S101 and $CH_3NH_3PbI_3$/spiro-OMeTAD.

recombination which suggests that S101 has slightly inferior charge extraction capability as compared to spiro-OMeTAD.

To further elucidate the low V_{oc} obtained from S101 devices, the charge-carrier dynamics at the perovskite/HTM interface and hole extraction ability were investigated using steady-state and time-resolved photoluminescence (PL) measurements, in which the efficient quenching of the steady-state PL and the reduction of the PL lifetime are indicators of efficient charge extraction at the perovskite/HTM interface. From the PL spectra (Fig. 4a), it is evident that both HTMs significantly quench the perovskite emission signal, with HTM spiro-OMeTAD having a slightly better PL quenching efficiency (*ca.* 93%) relative to S101 (*ca.* 89%). Time-resolved PL measurements were carried out with excitation at 404 nm and monitoring the entire emission spectral range (Fig. 4b). The pristine perovskite ($CH_3NH_3PbI_3$) exhibited a radiative lifetime of about 2.7 ns, whereas this was shorter in $CH_3NH_3PbI_3$/HTM samples. $CH_3NH_3PbI_3$/spiro-OMeTAD samples showed a decay time of 0.8 ns, whereas $CH_3NH_3PbI_3$/S101 samples showed a longer decay lifetime of 1.1 ns. This indicates that spiro-OMeTAD has slightly better hole extraction ability as compared to S101. As a result, it is unlikely that further device optimization will enable the device performance of S101 to exceed that of spiro-OMeTAD-based devices. The values of 11% and 12.3% obtained from our devices are below the current state-of-the-art values of over 20% but those result from extensive optimization of the perovskite preparation and device fabrication. We believe that with similar optimization efficiency, values close to 20% might be attainable using S101. In that case, the much lower cost of S101, due to its simpler synthesis and comparable device performance might offer a potentially lower cost/power ratio which is the ultimate economic criterion for photovoltaic systems.

Conclusions

A novel HTM S101 based silafluorene core has been synthesized *via* a short, low cost route and employed in a perovskite solar cell as a hole transporting layer. The devices fabricated with HTM S101 show a PCE of ~11% which is comparable to that (η = 12.3%) obtained with the state-of-the-art HTM spiro-OMeTAD. We firmly believe that with further optimization and fine tuning of various device parameters and by developing more understanding of interfacial characteristics, there can be further significant enhancement in the device performance. The short, efficient synthesis and good device performance mean that S101 has the potential to replace the more expensive spiro-OMeTAD. This work also lays out a strategy for the design and development of new cost effective and efficient HTMs for PSCs.

Acknowledgements

This work was funded by the National Research Foundation (NRF) Singapore (CRP Award no. NRF-CRP4-2008-03 and NRF-CRP14-2014-03), Singapore Ministry of Education (MOE2013-T2-044) and the Singapore-Berkeley Research Initiative for Sustainable Energy (SinBeRISE) CREATE Programme. Authors would like to thank Dr Francesco Maddalena for helping in fabricating FETs.

References

1 M. M. Lee, J. Teuscher, T. Miyasaka, T. N. Murakami and H. J. Snaith, *Science*, 2012, **338**, 643–647.
2 H. S. Kim, C.-R. Lee, J. H. Im, K.-B. Lee, T. Moehl, A. Marchioro, S.-J. Moon, R. Humphry-Baker, J.-H. Yum, J. E. Moser, M. Grätzel and N.-G. Park, *Sci. Rep.*, 2012, **2**, 591.
3 J. Burschka, N. Pellet, S.-J. Moon, R. Humphry-Baker, P. Gao, M. K. Nazeeruddin and M. Grätzel, *Nature*, 2013, **499**, 316–319.
4 T. Salim, S. Sun, Y. Abe, A. Krishna, A. C. Grimsdale and Y. M. Lam, *J. Mater. Chem. A*, 2015, **3**, 8943–8969.
5 A. Kojima, K. Teshima, Y. Shirai and T. Miyasaka, *J. Am. Chem. Soc.*, 2009, **131**, 6050–6051.
6 S. D. Stranks, G. E. Eperon, G. Grancini, C. Menelaou, M. J. P. Alcocer, T. Leijtens, L. M. Herz, A. Petrozza and H. J. Snaith, *Science*, 2013, **342**, 341–344.
7 G. Xing, N. Mathews, S. Sun, S. S. Lim, Y. M. Lam, M. Grätzel, S. Mhaisalkar and T. C. Sum, *Science*, 2013, **342**, 344–347.
8 H. Zhou, Q. Chen, G. Li, S. Luo, T.-b. Song, H.-S. Duan, Z. Hong, J. You, Y. Liu and Y. Yang, *Science*, 2014, **345**, 542–546.
9 N. J. Jeon, J. H. Noh, W. S. Yang, Y. C. Kim, S. Ryu, J. Seo and S. I. Seok, *Nature*, 2015, **517**, 476–480.
10 W. S. Yang, J. H. Noh, N. J. Jeon, Y. C. Kim, S. Ryu, J. Seo and S. I. Seok, *Science*, 2015, **348**, 1234.
11 Z. Yu and L. Sun, *Adv. Energy Mater.*, 2015, **5**(12), 1500213.
12 J. H. Heo, S. H. Im, J. H. Noh, T. N. Mandal, C.-S. Lim, J. A. Chang, Y. H. Lee, H.-j. Kim, A. Sarkar, M. K. Nazeeruddin, M. Grätzel and S. I. Seok, *Nat. Photonics*, 2013, **7**, 486–491.
13 H. Li, K. Fu, A. Hagfeldt, M. Grätzel, S. G. Mhaisalkar and A. C. Grimsdale, *Angew. Chem., Int. Ed.*, 2014, **53**, 4085–4088.
14 T. Krishnamoorthy, F. Kunwu, P. P. Boix, H. Li, T. M. Koh, W. L. Leong, S. Powar, A. Grimsdale, M. Grätzel, N. Mathews and S. G. Mhaisalkar, *J. Mater. Chem. A*, 2014, **2**, 6305–6309.

15 N. J. Jeon, J. Lee, J. H. Noh, M. K. Nazeeruddin, M. Grätzel and S. I. Seok, *J. Am. Chem. Soc.*, 2013, **135**, 19087–19090.
16 A. Krishna, D. Sabba, H. Li, J. Yin, P. P. Boix, C. Soci, S. G. Mhaisalkar and A. C. Grimsdale, *Chem. Sci.*, 2014, **5**, 2702–2709.
17 K. Do, H. Choi, K. Lim, H. Jo, J. W. Cho, M. K. Nazeeruddin and J. Ko, *Chem. Commun.*, 2014, **50**, 10971–10974.
18 P. Qin, S. Paek, M. I. Dar, N. Pellet, J. Ko, M. Grätzel and M. K. Nazeeruddin, *J. Am. Chem. Soc.*, 2014, **136**, 8516–8519.
19 B. Xu, E. Sheibani, P. Liu, J. Zhang, H. Tian, N. Vlachopoulos, G. Boschloo, L. Kloo, A. Hagfeldt and L. Sun, *Adv. Mater.*, 2014, **26**, 6629–6634.
20 H. Choi, S. Paek, N. Lim, Y. H. Lee, M. K. Nazeeruddin and J. Ko, *Chem.–Eur. J.*, 2014, **20**, 10894–10899.
21 A. Krishna, D. Sabba, J. Yin, A. Bruno, P. P. Boix, Y. Gao, H. A. Dewi, G. G. Gurzadyan, C. Soci, S. G. Mhaisalkar and A. C. Grimsdale, *Chem.–Eur. J.*, 2015, **21**, 15113–15117.
22 A. Abate, S. Paek, F. Giordano, J.-P. Correa-Baena, M. Saliba, P. Gao, T. Matsui, J. Ko, S. M. Zakeeruddin, K. H. Dahmen, A. Hagfeldt, M. Grätzel and M. K. Nazeeruddin, *Energy Environ. Sci.*, 2015, **8**, 2946–2953.
23 P. Gratia, A. Magomedov, T. Malinauskas, M. Daskeviciene, A. Abate, S. Ahmad, M. Grätzel, V. Getautis and M. K. Nazeeruddin, *Angew. Chem., Int. Ed.*, 2015, **54**, 11409–11413.
24 J. Liu, Y. Wu, C. Qin, X. Yang, T. Yasuda, A. Islam, K. Zhang, W. Peng, W. Chen and L. Han, *Energy Environ. Sci.*, 2014, **7**, 2963–2967.
25 M. Cheng, C. Chen, X. Yang, J. Huang, F. Zhang, B. Xu and L. Sun, *Chem. Mater.*, 2015, **27**, 1808–1814.
26 N. J. Jeon, H. G. Lee, Y. C. Kim, J. Seo, J. H. Noh, J. Lee and S. I. Seok, *J. Am. Chem. Soc.*, 2014, **136**, 7837–7840.
27 S. Ma, H. Zhang, N. Zhao, Y. Cheng, M. Wang, Y. Shen and G. Tu, *J. Mater. Chem. A*, 2015, **3**, 12139–12144.
28 S. Park, J. H. Heo, C. H. Cheon, H. Kim, S. H. Im and H. J. Son, *J. Mater. Chem. A*, 2015, **3**, 24215–24220.
29 H. Choi, K. Do, S. Park, J.-S. Yu and J. Ko, *Chem.–Eur. J.*, 2015, **21**, 15919–15923.
30 S. Yamaguchi and K. Tamao, *J. Chem. Soc., Dalton Trans.*, 1998, 3693–3702.
31 G. Lu, H. Usta, C. Risko, L. Wang, A. Facchetti, M. A. Ratner and T. J. Marks, *J. Am. Chem. Soc.*, 2008, **130**, 7670–7685.
32 J. Hou, H. Y. Chen, S. Zhang, G. Li and Y. Yang, *J. Am. Chem. Soc.*, 2008, **130**, 16144–16145.
33 Y. Sun, G. C. Welch, W. L. Leong, C. J. Takacs, G. C. Bazan and A. J. Heeger, *Nat. Mater.*, 2012, **11**, 44–48.
34 S. F. Chen, Y. Tian, J. Peng, H. Zhang, X. J. Feng, X. Xu, L. Li and J. Guo, *J. Mater. Chem. C*, 2015, **3**, 6822–6830.
35 C. Teng, X. Yang, C. Yang, S. Li, M. Cheng, A. Hagfeldt and L. Sun, *J. Phys. Chem. C*, 2010, **114**, 9101–9110.
36 C. M. Cardona, W. Li, A. E. Kaifer, D. Stockdale and G. C. Bazan, *Adv. Mater.*, 2011, **23**, 2367–2371.